The role of lattice distortions in determining the thermal properties of electron doped $CaMnO_3$

2009 J. Phys.: Condens. Matter 21 096001

(http://iopscience.iop.org/0953-8984/21/9/096001)

J. Phys.: Condens. Matter **21** (2009) 096001 (14pp) doi:10.1088/0953-8984/21/9/096001

The role of lattice distortions in determining the thermal properties of electron doped $CaMnO_3$

Archana Srivastava[1,2,3] **and N K Gaur**[1]

[1] Department of Physics, Barkatullah University, Bhopal 462026, India
[2] Department of Physics, Sri Sathya Sai College for Women, Bhopal-462024, India

E-mail: archanasaran@rediffmail.com

Received 25 September 2008, in final form 26 November 2008
Published 4 February 2009
Online at stacks.iop.org/JPhysCM/21/096001

Abstract

We have investigated the thermal properties of electron doped perovskite manganite $CaMnO_3$, the end member ($n = \infty$) of the Ruddlesden–Popper (RP) calcium manganates series with cation doping at the A-site. In this paper the functional relation between the lattice distortions and the thermal properties is determined and compared to available reports. The temperature dependence of the lattice specific heat ($C_{v(\text{lattice})}$) of $Ca_{1-x}Ln_xMnO_3$ ($x = 0.05, 0.10, 0.15, 0.20$) with Ln(= La, Ce, Pr, Nd, Th, Bi) doping at the A-site has been studied as a function of temperature ($10\ \text{K} \leqslant T \leqslant 500\ \text{K}$) by means of a rigid ion model (RIM) after modifying its framework to incorporate the van der Waals interactions. Strong electron–phonon interactions are present in these compounds, which are responsible for the variation of the lattice specific heat with cation doping of varying size and valency. We have found that the calculated thermal properties reproduce well the corresponding experimental data, implying that modified RIM represents properly the nature of these perovskite manganite systems. We demonstrate that the electron concentration, size mismatch and Jahn–Teller (JT) effects are the dominant factors, whereas charge mismatch and buckling of Mn–O–Mn angle influence the thermal properties to a lesser degree in the ferromagnetic state. In the insulating paramagnetic state, JT distortions vary linearly and influence the thermal properties. These specific heat results can be further improved by including the ferromagnetic spin wave and charge order contributions to the specific heat.

1. Introduction

The search for new magnetoresistive materials has commanded much attention for the past few years due to the enormous variety of fascinating physical properties exhibited. The need for new magnetic recording devices and an understanding of the phenomena at some fundamental level has provided a further impetus for the discovery of CMR and GMR materials. A great deal of work was devoted to the hole doped manganites with the perovskite structure in these last years, owing to their spectacular colossal magnetoresistance (CMR) properties. In contrast, very few investigations were performed on the electron doped manganites, corresponding to Mn(IV)-rich perovskites. Such compounds should be of great interest if one considers the magnetic and transport properties of the perovskites $Ca_{1-x}Bi_xMnO_3$, with x ranging from 0.25 to 0.10 [1] and non-saturated ferromagnetism of $Ca_{1-x}Sm_xMnO_3$ with $0 < x < 0.12$ [2]. Although electron doped manganites generally exhibit a smaller magnetoresistance ratio than their hole doped counterparts, the study of electron doped ones is important for the understanding of the mechanisms which govern the CMR properties.

Recently, Zeng *et al* [3] and Caspi *et al* [20] reported structural, magnetic and transport measurements for $Ca_{1-x}Ce_xMnO_3$ ($x = 0.2$) below 400 K. The results indicate that the formal oxidation state of cerium is Ce^{4+}, leading to mixed valence, Mn^{3+} and Mn^{4+}, in $CaMnO_3$. A large magnetoresistance was observed for the $Ca_{0.925}Ce_{0.075}MnO_3$ phase. The systematic exploration of

[3] Address for correspondence: Superconductivity Laboratory, Department of Physics, Barkatullah University, Bhopal, 462026, India.

the perovskites $Ca_{1-x}RE_xMnO_3$ and $Ca_{1-x}Th_xMnO_3$ [4] has shown that electron concentration is a predominant factor governing the CMR in these manganites.

$CaMnO_3$, the parent compound of electron doped colossal magnetoresistance materials, was studied a long time back by Yankel [5] and Wollan *et al* [6]; in comparison the study of electron doped manganites is a recent phenomenon. It is established that stoichiometric $CaMnO_3$ is antiferromagnetic insulator without e_g carriers and shows G-type spin ordering below T_N due to the inherent superexchange interaction between the neighbouring Mn^{4+} sites. The substitution of divalent cation Ca by trivalent or tetravalent ions (referred to as electron doping of the e_g orbital) leads to the simultaneous occurrence of Mn^{3+} and Mn^{4+} ions in the crystalline structure and significantly modifies the structural and transport properties of $CaMnO_3$, presenting complex phase diagrams including phases with different magnetic and charge order. With an increase of electron density n $(=x)$, an insulator–metal crossover is induced. Accordingly, the ferromagnetic component, which can be ascribed to the double-exchange interaction mediated by itinerant e_g carriers, is enhanced in the spin ordered phase. At the same time this doping (with Ln^{3+} or Th^{4+} cations) at the A-site introduces distortions in the cubic geometry of the compound and so these electron doped compounds are found to be orthorhombic within the *Pnma* space symmetry at low temperatures. The orthorhombic deformation of the cubic perovskite lattice is described in terms of rotation of MnO_6 octahedra of the so-called $GdFeO_3$ structure and the Jahn–Teller (JT) distortion. The JT distortion can be Q_2-mode (apically compressed along the b axis) or Q_3-mode (apically elongated) on either side of optimal x doping (corresponding to maximum magnetoresistance ratio). This cooperative JT deformation of the MnO_6 octahedron plays a vital role in determining the properties of these compounds.

Taking into consideration these results and the fact that the CMR properties may be highly sensitive to the carrier concentration, as demonstrated for the hole doped manganites, the $Ca_{1-x}Ln_xMnO_3$ manganites have been reinvestigated to study their thermal properties by varying x in the range $0.05 < x < 0.20$ for $Ln = La^{3+}$, Ce^{4+}, Pr^{3+}, Nd^{3+}, Th^{4+}, Bi^{3+}. As the electron concentration in these manganites is directly related to the valence of the doping element, only half the amount of Th(IV) or Ce(IV) (compared to Ln(III)) is necessary to reach the optimal CMR, i.e. $x = 0.15$ and 0.08 for $Ca_{1-x}Ln_xMnO_3$ and $Ca_{1-x}(Th/Ce)_xMnO_3$, respectively [7]. In the present investigation, depending on the size of the doped cation we have divided the case of cation doping at the A-site in $CaMnO_3$ manganites into two categories:

(a) when the doped ion radius is smaller (Ce, Nd, Th) and
(b) when the doped ion radius is larger (La, Bi) than or equal (Pr) to that of the parent Ca^{2+} ion.

To the best of our knowledge, no systematic investigation of thermal properties of these electron doped manganites has been carried out in the past, whereas it is well established that strong electron–phonon coupling is present in these compounds. This strong coupling is one of the most relevant contributions in determining the conduction mechanism in these manganites, and it can be affected by lattice distortions, substantially. Therefore, the study of the lattice thermal properties of these compounds may be taken as a starting point for the consistent understanding of the more complex physical properties of the electron doped manganites. The main focus of the present paper is on exploring the temperature dependence of the lattice specific heat of $CaMnO_3$ in the electron doped region of the phase diagram. Recently, we have successfully portrayed the thermodynamic and elastic properties of some manganites [11–15] by using a modified rigid ion model (MRIM). Motivated by the success and versatility of the model, we are exploring the thermal properties of $Ca_{1-x}Ln_xMnO_3$ ($Ln = La^{3+}$, Ce^{4+}, Pr^{3+}, Nd^{3+}, Th^{4+}, Bi^{3+}) for x varying from 0.05 to 0.2 using the modified RIM, and it is probably the first time that this has been done. The essentials of the MRIM formalism and the results obtained from its application are presented in subsequent sections.

2. Formalism of RIM

We have formulated the modified rigid ion model (MRIM) by keeping the effect of long-range (LR) Coulomb attractions, the short-range (SR) Hafemeister–Flygare-type (HF) [8] overlap repulsion effective up to the next nearest neighbour atoms and the van der Waals attraction due to dipole–dipole (d–d) interactions. The potential describing the formalism of MRIM is expressed as

$$\phi = \phi^{\mathrm{C}}_{kk'} + \phi^{\mathrm{R}}_{kk'} + \phi^{\mathrm{vdW}}_{kk'} \tag{1}$$

where the first term is the LR Coulomb attraction potential expressed as

$$\phi^{\mathrm{C}}_{kk'}(r) = -\frac{e^2}{2}\sum_{kk'} Z_k Z_{k'} r^{-1}_{kk'} \tag{2}$$

with $r_{kk'}$ as the separation between the two atoms designated k and k' and summation is performed over all the kk' ions. The overlap repulsive energy $\phi^{\mathrm{R}}_{kk'}(r)$ according to the Hafemeister–Flygare-type (HF) [8] interaction extended up to the second neighbour is expressed as

$$\begin{aligned}\phi^{\mathrm{R}}_{kk'}(r) = {} & \sum_i n_i b_i \beta_i^{kk'} \exp\{(r_k + r_{k'} - r_{kk'})/\rho_i\} \\ & + b_i n_i' \beta_i^{kk} \exp\{(2r_k - r_{kk})/\rho_i\} \\ & + b_i \frac{n_i''}{2} \beta_i^{k'k'} \exp\{(2r_{k'} - r_{k'k'})/\rho_i\}.\end{aligned} \tag{3}$$

Here $r_{kk'}$ appearing in the first term on the right represents the separation between the nearest neighbours while r_{kk} and $r_{k'k'}$ appearing in the following two terms are the second-neighbour separations. r_k ($r_{k'}$) is the ionic radius of the k (k') ion. n (n' and n'') is the number of nearest (next nearest) neighbour ions. In ABO_3 (like $CaMnO_3$) perovskite structure, k represents the cation (A, B) and k' denotes the type (O_1, O_2) of ion. The summation is performed over the ion pair (A–O) and (B–O). b_i and ρ_i are the hardness and range parameters for the ith cation–anion pair ($i = 1, 2$) respectively and $\beta_i^{kk'}$ is the Pauling coefficient [9] given by

$$\beta_i^{kk'} = 1 + \frac{Z_k}{N_k} + \frac{Z_{k'}}{N_{k'}} \tag{4}$$

Z_k ($Z_{k'}$) and N_k ($N_{k'}$) are the valence and the number of electrons in the outermost orbit of the k (k') ion respectively. The $r_{kk'}$, and r_{kk} and $r_{k'k'}$, are obtained for some doping concentration (x) of Ln = La, Ce, Pr, Nd, Th, Bi by using the well known Vegard law [24] using the cell parameters of undoped compounds like $CaMnO_3$ and $NdMnO_3$. The contribution of the van der Waals (vdW) attraction for the dipole–dipole interaction is determined by using the Slater–Kirkwood variational (SKV) method [10] and was defined in our earlier papers [11–15]:

$$\phi_{kk'}^{\mathrm{vdW}} = C_{kk'} r_{kk'}^{-6} \qquad \text{and}$$

$$C_{kk'} = \frac{3eh}{4\pi m}\alpha_k\alpha_k'\left[\left(\frac{\alpha_k}{N_k}\right)^{1/2} + \left(\frac{\alpha_{k'}}{N_k'}\right)^{1/2}\right]^{-1} \tag{5}$$

where e and m are the charge and mass of the electron respectively. α_k (α_k') is the polarizability of the k (k') ion. N_k (N_k') is the effective number of electrons responsible for the polarization of the k (k') ion.

The model parameters, hardness (b) and range (ρ), are determined from the equilibrium condition

$$\left[\frac{\mathrm{d}\phi}{\mathrm{d}r}\right]_{r=r_0} = 0 \tag{6}$$

and the bulk modulus

$$B = \frac{1}{9Kr_0}\left[\frac{\mathrm{d}^2\phi}{\mathrm{d}r^2}\right]_{r=r_0} \tag{7}$$

where K is the crystal structure-dependent constant and r_0 is the equilibrium nearest neighbour distance. The expressions for calculating the thermodynamic properties are taken from our earlier papers [11–15].

The model parameters obtained from the equations (6) and (7) have been used to compute the thermodynamic properties of the electron doped compounds. The cohesive energy for $Ca_{1-x}Ln_xMnO_3$ is calculated using equation (1) and other thermal properties like the molecular force constant (f), reststrahlen frequency (ν_0), and Debye temperature (θ_D), Grüneisen parameter (γ) and heat capacity are computed using the expression given in [12, 15]. The expression for the lattice specific heat is

$$C_{V\,(\mathrm{lattice})} = 9R\left(\frac{T}{\theta_D}\right)^3 \int_0^{\theta_D/T} \frac{\mathrm{e}^x x^4}{\mathrm{e}^x - 1}\mathrm{d}x. \tag{8}$$

And at the very low temperatures ($T < \theta_D/50$) the specific heat is calculated by using

$$C_{V\,(\mathrm{lattice})} = \frac{12\pi^4 p}{5}\left[Nk_B\left[\frac{T}{\theta_D}\right]^3\right] \tag{9}$$

where p is the number of atoms in one formula unit. N is the Avogadro number, k_B is the Boltzmann constant, R is the universal gas constant and θ_D is the Debye temperature. The Debye temperature (θ_D) is given by the expression

$$\theta_D = \frac{h\nu}{k_B} \tag{10}$$

with h as the Planck constant and ν as the reststrahlen frequency

$$\nu = \frac{1}{2\pi}\left[\frac{f}{\mu}\right]^{\frac{1}{2}} \tag{11}$$

where μ is the reduced mass and f is the molecular force constant given by

$$f = \frac{1}{3}\left[\phi_{kk'}^{\prime\prime\mathrm{SR}}(r) + \frac{2}{r}\phi_{kk'}^{\prime\mathrm{SR}}(r)\right]_{r=r_0} \tag{12}$$

with $\phi_{kk'}^{\mathrm{SR}}(r)$ the short-range nearest neighbour part of $\phi_{kk'}(r)$. The primes denote the first-order and second-order derivatives of the $\phi_{kk'}^{\mathrm{SR}}(r)$ with respect to the inter-ionic separation (r). We calculated the molecular force constant as a function of temperature, and the values of the Debye temperature and specific heat of the lattice over a fairly large interval of temperature follow. The Grüneisen parameter is calculated using the relation

$$\gamma = \frac{-r_0}{6}\left[\frac{\phi_{kk'}'''(r)}{\phi_{kk'}''(r)}\right]_{r=r_0} \tag{13}$$

where r_0 is the equilibrium distance between the k th and k'th ions and the primes in $\phi_{kk'}(r)$ denote the third-order and second-order derivatives of the $\phi_{kk'}(r)$ with respect to the inter-ionic separation (r). The results thus obtained are presented and discussed below.

3. Results and discussion

3.1. Model parameters

The values of input data like the unit cell parameters (a, b, c) and inter-ionic distances are taken from [1, 4, 7, 16–22] for the evaluation of model parameters (b_1, ρ_1) and (b_2, ρ_2) corresponding to the ionic pairs Mn^{3+}/Mn^{4+}–O^{2-} and $Ln^{3+/4+}/Ca^{2+}$–O^{2-} (Ln = La, Ce, Pr, Nd, Th, Bi) for different compositions x ($0.05 \leqslant x \leqslant 0.2$) and temperatures (10 K $\leqslant T \leqslant$ 500 K) for electron doped $Ca_{1-x}Ln_xMnO_3$. Taking the lattice parameter of $CaMnO_3$ [53] and other pure manganites $ReMnO_3$ [23], the well known Vegard law [24] is used to calculate the input lattice parameters for some compositions (x) of $Ca_{1-x}Ln_xMnO_3$ for which the experimental values are not available. The vdW coefficients $C_{kk'}$ were calculated using the SKV method [10] for the present manganites. The values of the model parameters (b_1, b_2, ρ_1 and ρ_2) for various compositions (x) of $Ca_{1-x}Ln_xMnO_3$ are listed in table 1. The decreasing trend of the hardness parameter b_1 for La, Pr and Th doping indicates the lesser distortion of the perfect octahedra of $CaMnO_3$ compared to Nd, Ce, Bi doping and subsequent decrease in the strength of the crystal with higher levels of doping. The hardness parameter b_2 for Ln^{3+}/Ca^{2+}–O^{2-} ion pairs increases for larger sized rare earth cation doping (La. Bi) while it decreases for equal or smaller cation doping (Pr, Nd). The Th^{4+} and Ce^{4+} doping is different from the above two cases; here b_2 increases for these doping concentrations. The range parameter ρ_1 of doped $CaMnO_3$ increases slightly (except for some concentrations of Th and Pr) with all kinds

Table 1. The A-site cation radius, tolerance factor and model parameters for orthorhombic $Ca_{1-x}Ln_xMnO_3$ compounds below the transition temperature T_N.

Compound	r_A (Å)	Tolerance factor t	$b_1 \times 10^{-19}$ (J) (Mn–O)	$b_2 \times 10^{-19}$ (J) (Ca/Ln–O)	ρ_1 (Å) (Mn–O)	ρ_2 (Å) (Ca/Ln–O)
$CaMnO_3$	1.180	0.945	0.847	0.797	0.287	0.442
$Ca_{0.75}La_{0.25}MnO_3$	1.189	0.935	0.803	1.158	0.293	0.516
$Ca_{0.80}La_{0.20}MnO_3$	1.187	0.937	0.807	1.133	0.292	0.509
$Ca_{0.83}La_{0.17}MnO_3$	1.186	0.938	0.807	1.126	0.290	0.506
$Ca_{0.87}La_{0.13}MnO_3$	1.185	0.940	0.825	1.141	0.291	0.506
$Ca_{0.90}La_{0.10}MnO_3$	1.184	0.941	0.837	1.152	0.291	0.506
$LaMnO_3$	1.216	0.905	0.719	1.090	0.314	0.542
$Ca_{0.80}Ce_{0.20}MnO_3$	1.150	0.923	0.902	1.353	0.312	0.556
$Ca_{0.85}Ce_{0.15}MnO_3$	1.158	0.929	0.885	1.340	0.306	0.548
$Ca_{0.90}Ce_{0.10}MnO_3$	1.165	0.934	0.868	1.324	0.299	0.539
$Ca_{0.95}Ce_{0.05}MnO_3$	1.173	0.940	0.850	1.312	0.292	0.532
$PrMnO_3$	1.179	0.892	0.617	0.551	0.292	0.411
$Ca_{0.82}Pr_{0.18}MnO_3$	1.180	0.935	0.811	0.792	0.290	0.447
$Ca_{0.86}Pr_{0.14}MnO_3$	1.180	0.937	0.804	0.785	0.288	0.444
$Ca_{0.90}Pr_{0.10}MnO_3$	1.180	0.940	0.795	0.775	0.285	0.441
$NdMnO_3$	1.162	0.886	0.576	0.512	0.283	0.394
$Ca_{0.80}Nd_{0.20}MnO_3$	1.176	0.933	1.048	0.760	0.318	0.440
$Ca_{0.85}Nd_{0.15}MnO_3$	1.177	0.936	1.071	0.770	0.319	0.441
$Ca_{0.90}Nd_{0.10}MnO_3$	1.178	0.939	1.094	0.779	0.319	0.441
$Ca_{0.80}Th_{0.20}MnO_3$	1.162	0.928	0.729	1.095	0.289	0.506
$Ca_{0.85}Th_{0.15}MnO_3$	1.167	0.932	0.747	1.103	0.287	0.504
$Ca_{0.90}Th_{0.10}MnO_3$	1.171	0.936	0.761	1.107	0.285	0.501
$Ca_{0.95}Th_{0.05}MnO_3$	1.176	0.941	0.774	1.109	0.283	0.497
$Ca_{0.80}Bi_{0.20}MnO_3$	1.192	0.938	0.876	0.909	0.298	0.473
$Ca_{0.85}Bi_{0.15}MnO_3$	1.189	0.940	0.872	0.916	0.296	0.471
$Ca_{0.90}Bi_{0.10}MnO_3$	1.186	0.942	0.852	0.917	0.292	0.468

of doping whereas ρ_2, being more sensitive (as the doping is only at the A-site which affects the Ln^{3+}/Ca^{2+}–O^{2-} pair predominantly), decreases only for the smaller sized rare earth cation doping (Nd^{3+}) and remains almost unaffected by the same size cation Pr^{3+}.

3.2. Cohesive properties

We calculated the cohesive energies of $Ca_{1-x}Ln_xMnO_3$ compounds using equation (1) and reported them in tables 3 and 4. The negative values of the cohesive energy indicate the stabilities of these compounds. It has been noticed while calculating the values of the cohesive energy using equation (1) that the contribution from the short-range repulsion is less than 10% of the total cohesive energy and the van der Waals term contributes around 5%. The experimental values of the cohesive energy for $Ca_{1-x}Ln_xMnO_3$ are not available, but our calculated values are close to the reported values −139.70 eV and −146.2 eV for the compounds $LaMnO_3$ [25] and $PrMnO_3$ [26] manganites, respectively. To test the validity of our model, we calculated the lattice energies of these compounds using the generalized Kapustinskii equation [27] which uses the ionic strength of the crystal defined as

$$I = -(1/2)\sum_{k}^{t} n_k z_k^2 \qquad (14)$$

where t is the number of the type of ions in the formula unit, each of number n_k and charge z_k. In our calculations the value of the ionic strength for the $CaMnO_3$ compound is found to be 16 and this value decreases slightly due to cation doping at the A-site. According to the generalized Kapustinskii equation the lattice energies of crystals with multiple ions are given as

$$U\,(\mathrm{kJ\ mol^{-1}})^{-1} = -\frac{1213.9}{\langle r\rangle}\left(1-\frac{\rho}{\langle r\rangle}\right)\sum n_k z_k^2 \qquad (15)$$

where $\langle r\rangle$ is the weighted mean cation–anion radius sum (using Goldschmidt radii) and ρ is taken as the average of our model parameters ρ_1 and ρ_2. The value of the lattice energy of the compounds as estimated using the empirical Kapustinskii equation is found to be in good agreement with our calculated values, giving further confidence in the validity of our model (the average deviation is less than 2%). It can be inferred from the results for the cohesive energy (table 3) that the stability of doped compounds is somewhat less compared to that of the parent compound, and this can be correlated with the observed distortions of the lattice compared to the parent compound. Analysing the results on cohesive energy in the paramagnetic phase (table 4) shows that the stability of these compounds has enhanced in this phase compared to spin ordered phase (ferromagnetic or antiferromagnetic) (table 3). Recently, the Madelung energy of the valence skip compound $BaBiO_3$ with perovskite structure was reported to be around −165 eV (which is the first term of our equation (1)) [55].

3.3. Bulk modulus

The value of the bulk modulus for the compounds under investigation is an important input parameter from the point of view of critical determination of model parameters, but the experimental values of the bulk modulus of $Ca_{1-x}Ln_xMnO_3$ are not available in the literature for most of the compounds and a few available values for the same compound show large deviations, as reported by various investigators; e.g. the value of the bulk modulus of $LaMnO_3$ was reported to be 85.4 GPa [28], 95.9 GPa [29], 108 GPa [30], 118.7 GPa [31], 123 GPa [32], 133 GPa [33], 143 GPa [34] and 182 GPa [54], which makes the choice of the bulk modulus value as input parameter a difficult task. So we thought of making a study of the determination of the bulk modulus of the $ReMnO_3$ (Re = rare earth) and the diluted compounds systematically, on the basis of formulations of atoms in molecules theory.

An interesting application of the atoms in molecules theory (AIM) is the partitioning of static thermodynamic properties in condensed systems; this has successfully predicted the compressibility of various halides and spinels [35]. The theory predicts that the bulk properties of any complex compound can be partitioned into the properties of its constituent groups/atoms. Since all AIM atomic properties are additive and quantum atoms fill the space, bulk or thermodynamic properties may be partitioned into atomic or group contributions. We have considered that the molar volume V can be written as the sum over atomic volumes (V_i) such that atomic volumes fill up the entire space of the lattice within the given structure and space symmetry. Hence, it was stated that the inverse of the bulk modulus is the simple weighted average of the atomic compressibilities [35]:

$$\kappa = \sum_i f_i \kappa_i \qquad \text{and} \qquad \frac{1}{B} = \sum_i f_i \frac{1}{B_i} \qquad \text{where } f_i = V_i/V \tag{16}$$

where f_i is the fractional volume occupancy due to quantum subsystem i in a unit formula volume, B is the bulk modulus of the compound and K is its compressibility. Here, we have considered oxygen atoms as the bulkiest and most compressible, and the local compressibility varies according to the varying cation volumes and their relative occupation factor f_i, along the lines of Pendas *et al* [35]. The oxide ions are plastic constituents of these structures. The values of the ionic radii are taken from [36] and the data on atomic compressibility from [37]. The compounds under study are all manganite perovskites and the lattice space is dominated by the MnO_6 octahedra with relatively small cations at the A-site. As proposed by Pendas *et al* [35], to a large extent the polyhedral bulk modulus is constant, so we expect all the bulk moduli of these compounds to cluster around some common value which is near the polyhedral bulk modulus. We have computed the bulk modulus using equation (16) on the basis of AIM theory and in this analysis the octahedra are considered to be undistorted and perfect. The values obtained by us are represented as B_0 in table 2. The bulk moduli calculated on the basis of AIM theory are found to be in good agreement with the experimental data (table 2). The calculated value of 75.6 GPa for $CaMnO_3$ is comparable to the value of 66.5 GPa reported by Buch *et al* [29]. The calculated value for $LaMnO_3$ is 103.43 GPa which is close to two reported values—95.9 GPa [29] and 108 GPa [30]. The calculated value of 80.43 GPa for $Ca_{0.8}La_{0.2}MnO_3$ is close to the value of 85 GPa at 60 K reported by Zhu *et al* [38].

Within the perovskite structure, Re^{3+} occupies the centre of the dodecahedron of oxygen. But due to orthorhombic deformation of the lattice, the coordination number of Re^{3+} reduces to 9, as three oxygen atoms remain essentially non-bonded. So we have considered the ionic radii of A-site cations of coordination number 9, from [36]. Now, if in this environment the Re^{3+} is substituted by a smaller cation, the dodecahedron of oxygen will try to collapse towards the central Re^{3+} cation and in turn the Mn–O–Mn angle will buckle. If we investigate the rare earth manganites $ReMnO_3$ (Re = La–Nd) where the A-site cation radius reduces down the series, the buckling of the Mn–O–Mn angle progressively increases, which leads to increased distortions of the lattice. As the cation radius decreases down the series, the tolerance factor t ($t = (r_A + r_O)/\sqrt{2}(r_B + r_O)$), whose value for $CaMnO_3$ quasicubic perovskite structure is around 1, also reduces (table 1), so the structure progressively deviates from the quasicubic to the orthorhombic form and a decrease in the unit cell volume can be observed. This decrease in cell volume corresponds to an increase in bulk modulus of the compound. So, the effect of decreasing the superexchange angle Mn–O–Mn ($\langle\theta\rangle$) from its ideal value of 180° for cubic perovskite (or increasing the tilt angle ($\langle\omega\rangle$) of the MnO_6 octahedra around the pseudocubic direction [111]) is to increase the bulk modulus of the compound. It can now be visualized that the buckling of the Mn–O–Mn angle due to substitution of a smaller cation at the A-site can substantially increase the bulk modulus of the compound as the tilting of the octahedra with decreasing cation size at the A-site will fill the unit cell volume effectively. This is evident from our results depicted in table 3 and in figure 1; the bulk modulus of $NdMnO_3$ is greater than that of $PrMnO_3$ which in turn is greater than the $LaMnO_3$ value. These results are near the earlier reports [42]. At the same time, the Debye temperature is expected to increase as well down the series from $LaMnO_3$ to $NdMnO_3$ (table 3).

When we consider the doping at the A-site in $ReMnO_3$ compounds, then the local compressibilities of impurities with respect to host ions are governed by the size difference and tuned by the formal charge mismatch between host and guest cations. We considered the effect of charge and size mismatch along with the octahedral distortions due to the Jahn–Teller effect on the bulk modulus of the compounds. These factors will determine the change in the unit cell volume, which in turn will change the global bulk modulus of the compound. The formal expression for calculating the JT distortion of BO_N octahedra is taken as

$$\Delta_{JT} = \sqrt{(1/N)\sum_i^N ((d_i - \langle d\rangle)/\langle d\rangle)^2} \tag{17}$$

where $\langle d\rangle$ is the average value of the d_i bond distances in BO_N octahedra. This distortion is found to be very small

Table 2. A-site variance, lattice distortions and bulk modulus (based on AIM theory) for $Ca_{1-x}Ln_xMnO_3$ manganites.

Compounds	Variance (A-site) σ^2 (Å^2)	B_O (GPa) (AIM)	JT distortion $\Delta_{JT} \times 10^{-3}$	Charge mismatch σ_C	Size mismatch σ_m	Octahedra rotation ϕ_S
$CaMnO_3$	0.00	75.61	1.747	0.500	2.226	0.982
Earlier reports		66.5[a]				
$Ca_{0.75}La_{0.25}MnO_3$	2.43	81.48	16.086	0.600	2.128	0.980
$Ca_{0.80}La_{0.20}MnO_3$	2.07	80.34	13.218	0.579	2.147	0.981
Earlier reports		85[b]				
$Ca_{0.83}La_{0.17}MnO_3$	1.83	79.67	11.497	0.567	2.158	0.981
$Ca_{0.87}La_{0.13}MnO_3$	1.47	78.67	9.203	0.550	2.174	0.981
$Ca_{0.90}La_{0.10}MnO_3$	1.17	77.96	7.482	0.538	2.186	0.981
$LaMnO_3$	0.00	103.43	59.104	1.000	1.885	0.977
Earlier reports		84.6[c]				
		95.9[a]				
$Ca_{0.80}Ce_{0.20}MnO_3$	36.00	85.51	3.575	0.667	2.080	0.981
$Ca_{0.85}Ce_{0.15}MnO_3$	28.69	83.18	3.700	0.622	2.115	0.981
$Ca_{0.90}Ce_{0.10}MnO_3$	20.25	80.93	3.862	0.579	2.151	0.981
$Ca_{0.95}Ce_{0.05}MnO_3$	10.69	78.66	1.504	0.538	2.189	0.982
$PrMnO_3$	0.00	119.15	56.925	1.000	1.828	0.968
$Ca_{0.82}Pr_{0.18}MnO_3$	0.00	81.25	11.679	0.571	2.142	0.979
$Ca_{0.86}Pr_{0.14}MnO_3$	0.00	80.15	9.471	0.554	2.161	0.980
$Ca_{0.90}Pr_{0.10}MnO_3$	0.00	79.11	7.264	0.538	2.179	0.980
$NdMnO_3$	0.00	124.37	68.425	1.000	1.802	0.966
$Ca_{0.80}Nd_{0.20}MnO_3$	0.52	82.81	15.082	0.579	2.127	0.979
$Ca_{0.85}Nd_{0.15}MnO_3$	0.41	80.92	11.748	0.558	2.151	0.980
$Ca_{0.90}Nd_{0.10}MnO_3$	0.29	79.10	8.414	0.538	2.176	0.980
$Ca_{0.80}Th_{0.20}MnO_3$	12.96	88.01	13.218	0.667	2.101	0.981
$Ca_{0.85}Th_{0.15}MnO_3$	10.33	84.75	10.350	0.622	2.132	0.981
$Ca_{0.90}Th_{0.10}MnO_3$	7.29	81.67	7.482	0.579	2.163	0.981
$Ca_{0.95}Th_{0.05}MnO_3$	3.85	78.69	4.614	0.538	2.194	0.981
$Ca_{0.80}Bi_{0.20}MnO_3$	5.76	80.67	5.625	0.579	2.156	0.981
$Ca_{0.85}Bi_{0.15}MnO_3$	4.59	79.32	5.625	0.558	2.173	0.981
$Ca_{0.90}Bi_{0.10}MnO_3$	3.24	78.07	7.056	0.538	2.190	0.981

[a] Reference [29], [b] Reference [38], [c] Reference [28].

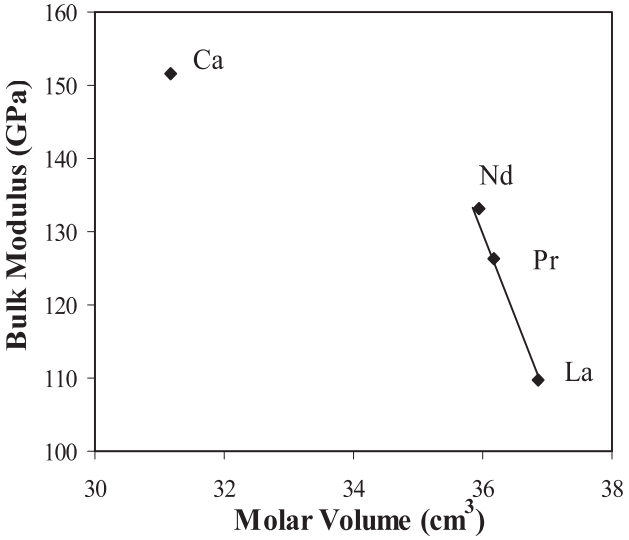

Figure 1. Bulk modulus of $CaMnO_3$, $ReMnO_3$ (Re = La, Pr, Nd) versus the molar volume of the basic perovskite cell. The solid line is a guide, to depict the linear variation.

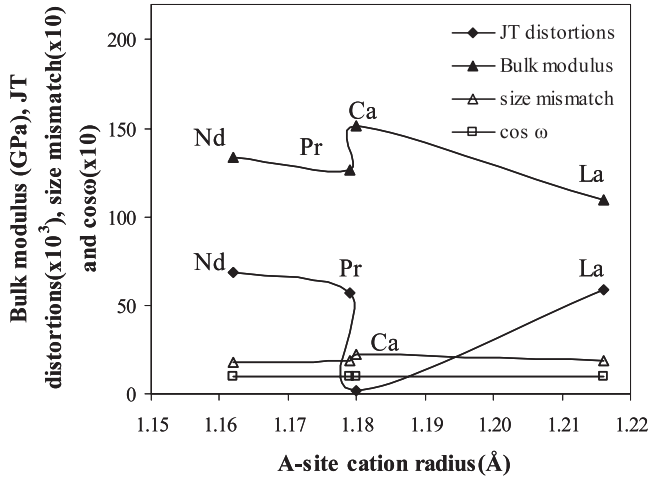

Figure 2. Variation of the octahedral distortion due to buckling of the superexchange Mn–O–Mn angle ($\cos\omega$), size mismatch, bulk modulus and JT distortions of $CaMnO_3$ and $ReMnO_3$ (Re = La–Nd) compounds with the radius of the A-site cation.

for MnO_6 octahedra, and is reported in table 2. We expect the bulk modulus to vary inversely with JT distortions; higher distortions of MnO_6 octahedra will mean a lower value of the bulk modulus of the compound (figure 3(a)). As this distortion decreases with lowering temperatures, the bulk modulus will slightly increase as we go towards lower temperatures from T_N.

Table 3. Bulk modulus, cohesive and thermal properties of orthorhombic $Ca_{1-x}Ln_xMnO_3$ at low temperatures (below the transition temperature T_N).

Compound	Bulk modulus B (GPa)	Φ (eV) (MRIM)	Φ (eV) (Kapustinskii equation)	f (N m^{-1})	ν (THz)	Θ_D (K)	γ
$CaMnO_3$	151.49	−156.25	−154.82	29.44	12.46	596.65	2.53
Earlier reports	147[a]						2–3[b]
$Ca_{0.75}La_{0.25}MnO_3$	138.01	−150.46	−148.05	26.38	10.50	502.81	2.45
$Ca_{0.80}La_{0.20}MnO_3$	140.61	−151.44	−149.09	26.87	10.82	518.30	2.46
$Ca_{0.83}La_{0.17}MnO_3$	141.87	−152.04	−149.67	27.15	11.02	527.95	2.47
$Ca_{0.87}La_{0.13}MnO_3$	144.18	−152.79	−150.17	27.40	11.27	539.99	2.47
$Ca_{0.90}La_{0.10}MnO_3$	145.87	−153.35	−150.57	27.60	11.47	549.62	2.47
$LaMnO_3$	109.72	−137.33	−136.61	21.77	7.48	358.07	2.42
Earlier reports	108[c]	−139.7[d]			8.58[e]	302[f]	
						369[g]	
$Ca_{0.80}Ce_{0.20}MnO_3$	128.72	−149.31	−146.71	24.31	10.28	492.43	2.32
$Ca_{0.85}Ce_{0.15}MnO_3$	134.30	−150.77	−147.87	25.26	10.72	513.30	2.36
$Ca_{0.90}Ce_{0.10}MnO_3$	140.33	−152.24	−149.08	26.28	11.19	536.04	2.40
$Ca_{0.95}Ce_{0.05}MnO_3$	146.31	−153.71	−150.23	27.30	11.69	559.89	2.44
$PrMnO_3$	126.25	−141.35	−143.40	26.10	8.16	390.95	2.68
Earlier reports	164[a]	−146.2[h]					
$Ca_{0.82}Pr_{0.18}MnO_3$	144.08	−153.34	−152.22	28.27	11.18	535.59	2.51
$Ca_{0.86}Pr_{0.14}MnO_3$	145.97	−153.93	−152.94	28.64	11.46	548.99	2.53
$Ca_{0.90}Pr_{0.10}MnO_3$	148.01	−154.53	−153.70	29.05	11.76	563.47	2.55
$NdMnO_3$	133.17	−142.48	−144.66	27.50	8.34	399.31	2.76
$Ca_{0.80}Nd_{0.20}MnO_3$	145.20	−152.71	−151.15	27.66	10.94	524.16	2.49
$Ca_{0.85}Nd_{0.15}MnO_3$	146.62	−153.41	−151.69	27.82	11.23	537.83	2.49
$Ca_{0.90}Nd_{0.10}MnO_3$	148.14	−154.13	−152.25	28.00	11.54	552.62	2.48
$Ca_{0.80}Th_{0.20}MnO_3$	133.77	−150.60	−149.81	26.20	10.33	494.59	2.44
$Ca_{0.85}Th_{0.15}MnO_3$	137.76	−151.79	−150.51	26.77	10.75	514.85	2.45
$Ca_{0.90}Th_{0.10}MnO_3$	142.12	−153.00	−151.28	27.43	11.22	537.58	2.47
$Ca_{0.95}Th_{0.05}MnO_3$	146.82	−154.26	−152.09	28.13	11.75	562.86	2.49
$Ca_{0.80}Bi_{0.20}MnO_3$	140.13	−152.24	−150.85	27.15	10.58	506.64	2.46
$Ca_{0.85}Bi_{0.15}MnO_3$	142.83	−153.13	−151.54	27.57	10.96	525.03	2.47
$Ca_{0.90}Bi_{0.10}MnO_3$	146.02	−154.11	−152.42	28.16	11.41	546.67	2.49

[a] Reference [42], [b] Reference [44], [c] Reference [30], [d] Reference [28], [e] Reference [45]; [f] Reference [46]; [g] Reference [47]; [h] Reference [26].

The change in bulk modulus will vary according to $T_N - T$. Above T_N the effect of JT distortions is to increase the value of bulk modulus. So we expect a minimum in the vicinity of the magnetic transition. Figure 2 depicts the inverse relation of bulk modulus and JT distortions of $CaMnO_3$ and $ReMnO_3$ (Re = La–Nd). The same inverse relation is observed in electron doped compounds as well (figure 3(a)).

The expressions for the cation size and charge mismatch at the A-site and B-site are

$$\sigma_m = \left[\frac{(1-x_A)r_A + x_A r_{A'}}{(1-x_A)r_{Mn^{3+}} + x_A r_{Mn^{4+}}}\right] \tag{18}$$

where x_A is the concentration of the doped cation of radius $r_{A'}$ (CN = 9) at the A-site and r_A is the radius of the Ca^{2+} cation (CN = 9). $r_{Mn^{3+}}$ (CN = 6) is the radius of the Mn^{3+} ion in valence state III and $r_{Mn^{4+}}$ (CN = 6) is the value for valence state IV. Similarly replacing the radius r_A ($r_{A'}$) with Ca^{2+} ($Ln^{3+/4+}$) charge at the A-site and r_{Mn} with the valence of Mn^{3+} and Mn^{4+} at the B-site, the charge mismatch can also be calculated (table 2). The variation of the bulk modulus of $Ca_{1-x}La_xMnO_3$ with charge and size mismatch at the A-site is given in figures 3(b) and (c). Similar variation is observed for other electron doped compounds as well.

The effect of buckling of the superexchange angle Mn–O–Mn on distortions of the unit cell is accounted for via

$$\phi_S = \cos\langle\omega\rangle = \cos\left(\pi - \langle\theta\rangle\right)/2 \tag{19}$$

where the average tilting of the BO_6 octahedra around the pseudocubic direction [111] is $\langle\omega\rangle$ and $\langle\theta\rangle$ is the average superexchange angle Mn–O–Mn.

The variations of the bulk modulus with these distortions are given for $Ca_{1-x}La_xMnO_3$ in figure 3. Similar variation for other electron doped compounds can be observed from table 3. The values of various distortions are also given in table 2. It is now appropriate to propose the following relation for the bulk modulus of the distorted perovskite manganite:

$$B_T = \frac{K_S B_0 \sigma_m \cos\omega}{\exp\left(\Delta_{JT}\right)\sigma_C} \tag{20}$$

where K_S is the spin order-dependent constant of proportionality, and its value is less than 1 for the ferromagnetic state and more than 1 for the paramagnetic state, B_0 is the bulk modulus for undistorted structure calculated on the basis of AIM theory, σ_m is the size mismatch, σ_C is the charge mismatch, Δ_{JT}

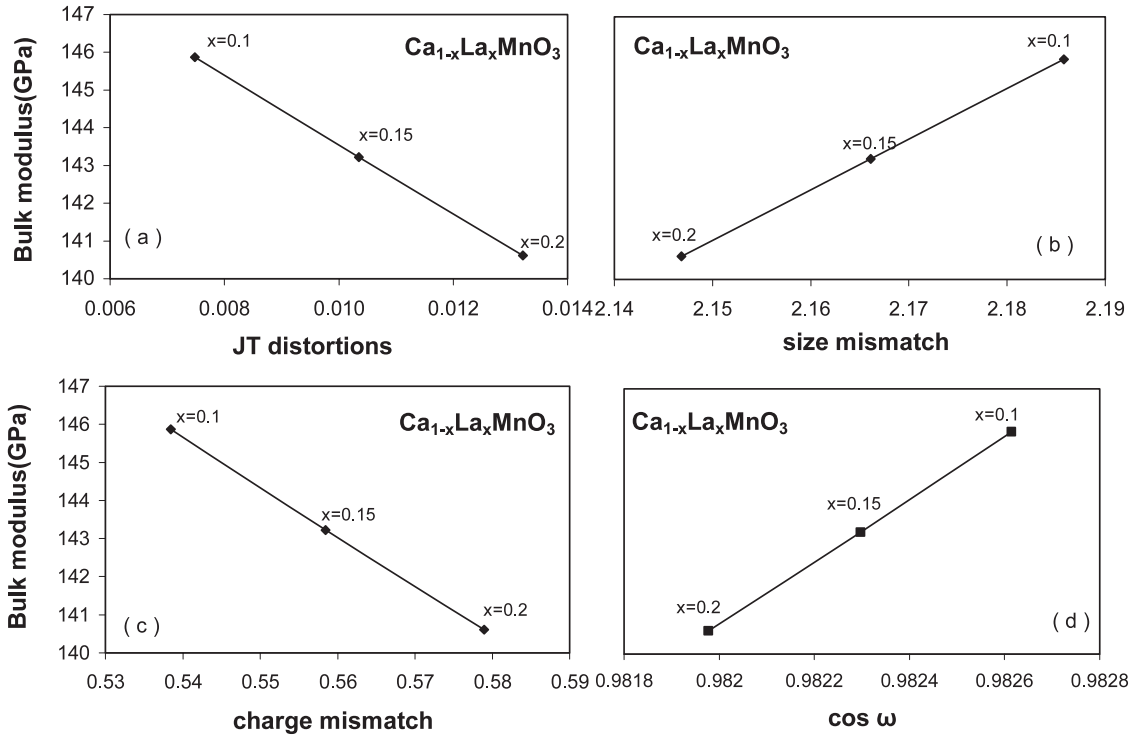

Figure 3. Relation of the bulk modulus to (a) JT distortions, (b) size mismatch, (c) charge mismatch (at the A-site) and (d) octahedral distortion due to buckling of the superexchange Mn–O–Mn angle ($\cos\omega$) in $Ca_{1-x}La_xMnO_3$ compounds.

is JT distortion of MnO_6 octahedra and $\cos\omega$ is the effect of buckling of the Mn–O–Mn angle. The value of the bulk modulus of the distorted structure is presented in table 4 as B_T. It can be observed from the table 4 that distortions change the bulk modulus B_0 by a factor of approximately 2–3 in insulating paramagnetic phase and the calculated value after considering the effect of various distortions is seemingly high compared to previous reports. We report the bulk modulus of $LaMnO_3$ in its insulating paramagnetic phase as 212 GPa and similar high values of bulk modulus were reported by several researchers in the past. This value is close to the value of 182 GPa reported by Youn *et al* [54] and 190 GPa for $LaTiO_3$ [39] (table 4). The calculated value of the bulk modulus of $CaMnO_3$ is 255 GPa and is close to the 211 GPa reported by Youn *et al* [54]. The value for $Ca_{0.8}La_{0.2}MnO_3$ is 220 GPa and this value is close to the reported value of 235 GPa for $La_{0.67}Ca_{0.33}MnO_3$ obtained by fitting the volume compressibility data to the Birch–Murnaghan equation of state [40].

We have displayed the variation of the bulk modulus of electron doped compounds as a function of molar volume in figure 4 and the bulk modulus is observed to be decreasing with increasing basic perovskite molar cell volume. Similar variation of the bulk modulus with the cell volume was observed previously also by Zimmer *et al* and recently by Shein *et al* for alkaline earth chalcogenides, ionic halides and transition metal diborides [41]. For each type of doped ion a linear variation is observed but with a different slope. Here, it is interesting to note that the slopes of trivalent cation (La, Pr, Nd, Bi) doped compounds are different from those for the tetravalent compounds (Th, Ce) and the slopes for La, Nd and Bi doped compounds are approximately the same. The natures

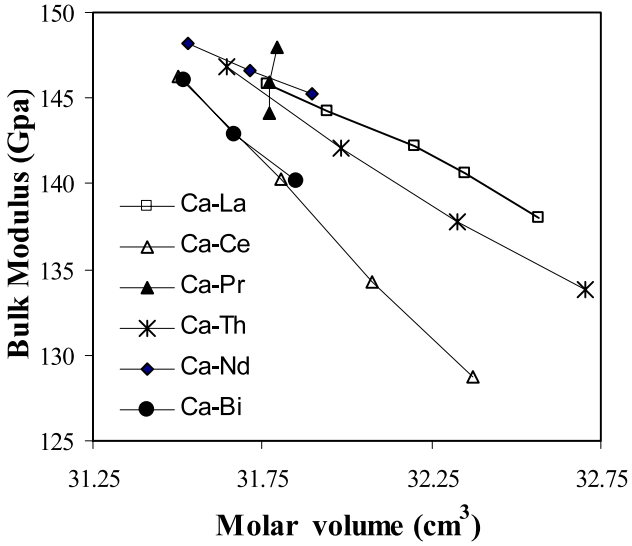

Figure 4. Variation of the bulk modulus of electron doped compounds with the molar volume of the basic perovskite cell.

of the curves for Th and Ce doping are also similar, these both being tetravalent impurities. For praseodymium (Pr) doping in $CaMnO_3$, the cation size variance at the A-site is nearly zero and the experimentally observed cell volumes are nearly constant; also it can be noticed from figure 4 that the slope of this curve is different from those of all other curves, and is the highest too. The reason appears to be its minimum cation size variance. The slope of the La, Nd, Bi doped series curves decreases as the variance increases, from La to Bi

Table 4. Bulk modulus, cohesive and thermal properties of orthorhombic $Ca_{1-x}Ln_xMnO_3$ manganites in the insulating paramagnetic phase.

Compound	B_T (GPa)	Φ (eV)(MRIM)	Φ (eV) (Kapustinskii equation)	f (N m^{-1})	ν (THz)	Θ_D (K)	γ
$CaMnO_3$	255.00	−165.94	−164.59	49.56	16.16	774.10	3.53
Earlier reports	211[a]						
$Ca_{0.75}La_{0.25}MnO_3$	204.22	−157.90	−156.01	39.04	12.77	611.65	3.13
$Ca_{0.80}La_{0.20}MnO_3$	220.29	−159.89	−158.07	42.07	13.54	648.56	3.27
Earlier reports	235[b]					650[c]	
$Ca_{0.83}La_{0.17}MnO_3$	224.62	−160.74	−158.68	42.76	13.83	662.53	3.28
$Ca_{0.87}La_{0.13}MnO_3$	231.54	−161.73	−159.63	43.94	14.28	683.88	3.32
$Ca_{0.90}La_{0.10}MnO_3$	236.77	−162.49	−160.30	44.80	14.62	700.24	3.35
$LaMnO_3$	211.81	−148.21	−148.67	42.03	10.39	497.50	3.69
Earlier reports	190[d]	−139.7[e]				470,	
	182[a]					515[f]	
$Ca_{0.80}Ce_{0.20}MnO_3$	190.00	−157.00	−155.10	35.88	12.49	598.26	2.95
$Ca_{0.85}Ce_{0.15}MnO_3$	205.07	−159.05	−156.88	38.57	13.24	634.28	3.06
$Ca_{0.90}Ce_{0.10}MnO_3$	221.69	−161.08	−158.69	41.52	14.07	673.76	3.19
$Ca_{0.95}Ce_{0.05}MnO_3$	239.18	−163.12	−160.42	44.63	14.94	715.86	3.32
$PrMnO_3$	236.30	−151.08	−153.51	48.84	11.17	534.85	4.05
Earlier reports		−146.2[g]					
$Ca_{0.82}Pr_{0.18}MnO_3$	225.71	−161.72	−160.68	44.29	13.99	670.36	3.34
$Ca_{0.86}Pr_{0.14}MnO_3$	231.77	−162.52	−161.62	45.47	14.44	691.76	3.39
$Ca_{0.90}Pr_{0.10}MnO_3$	238.92	−163.36	−162.66	46.90	14.95	715.89	3.46
$NdMnO_3$	48.39	−151.96	−154.49	51.30	11.38	545.34	4.18
$Ca_{0.80}Nd_{0.2}MnO_3$	223.76	−161.25	−160.39	43.84	13.78	650.69	3.33
$Ca_{0.85}Nd_{0.15}MnO_3$	230.92	−162.40	−161.42	45.15	14.30	674.95	3.37
$Ca_{0.90}Nd_{0.1}MnO_3$	238.48	−163.56	−162.46	46.54	14.87	701.15	3.42
$Ca_{0.80}Th_{0.20}MnO_3$	200.76	−158.31	−157.99	39.32	12.65	605.91	3.15
$Ca_{0.85}Th_{0.15}MnO_3$	212.71	−160.03	−159.23	41.34	13.36	639.75	3.22
$Ca_{0.90}Th_{0.10}MnO_3$	225.80	−161.76	−160.53	43.58	14.15	677.61	3.31
$Ca_{0.95}Th_{0.05}MnO_3$	240.08	−163.52	−161.85	46.00	15.03	719.75	3.40
$Ca_{0.80}Bi_{0.20}MnO_3$	221.64	−160.56	−159.77	43.13	13.33	637.31	3.31
$Ca_{0.85}Bi_{0.15}MnO_3$	229.22	−161.78	−160.66	44.36	13.90	664.72	3.35
$Ca_{0.90}Bi_{0.10}MnO_3$	237.30	−163.07	−161.67	45.86	14.56	694.90	3.40

[a] Reference [54]; [b] Reference [40]; [c] Reference [49]; [d] Reference [39]; [e] Reference [25]; [f] Reference [48, 11]; [g] Reference [26].

doping compounds. It further decreases progressively from the Ca–Th series compounds to the Ca–Ce series (with maximum variance). So, the slope of these curves seems to be inversely proportional to the A-site cation variance:

$$\partial B/\partial r_A \propto 1/\sigma_A^2. \quad (21)$$

This simply implies that if the size of the doped ion is very much different from that of the parent compound A-site ion (Ca) (i.e. high A-site variance σ_A^2), then the variation of the bulk modulus with the molar volume will be slower. This size-dependent effect seems to be independent of the number of electrons doped in the e_g orbital of the parent compound, i.e. the valence of the doped element.

3.4. Thermal properties

We have also computed the molecular force constant f, reststrahlen frequency ν_0, Debye temperature θ_D and Grüneisen parameter γ in the low temperature regime, below the magnetic transition temperature for these electron doped compounds, and results are reported in table 3. These values can be compared with the calculated values for the parent compound $CaMnO_3$ given in table 3, revealing clearly the large effect of electron doping on the thermal properties of $CaMnO_3$. The value of the Grüneisen parameter below the transition temperature T_N seems to be reasonable since its value lies between 2 and 3 as reported earlier [44]. In the Debye approach we consider the vibrations of the collective positive ion lattice with respect to the negative ion lattice. The frequency of vibration obtained from this model is also reported here as the reststrahlen frequency. It is clear from table 3 that doping with rare earth cations (La–Nd), Bi^{3+} and Th^{4+} decreases the reststrahlen frequency of the compound $CaMnO_3$. The reststrahlen frequency for these compounds is close to the reported value of 8.58 THz for $LaMnO_3$ [45], but our comments on the reliability of these values must be limited until reports of experimental data for these compounds appear.

It is to be noted that the high value of the Debye temperature indicates higher phonon frequencies for these doped compounds. The calculated values of the Debye temperature are compared with the available experimental data in table 3 and 4 but it is interesting to note that our low temperature θ_D (table 3) are comparable to the Debye temperatures often observed for perovskite oxides of ABO_3-

type structure. Our calculated value of 358 K for the Debye temperature of $LaMnO_3$ is close to the reported values of 302 K [46] and 369 K for oxygen deficient $LaMnO_3$ from Ghivelder *et al* [47]. Our HT θ_D is 497 K and it is close to the reported value of 470 K of Talati *et al* [48]. For $Ca_{1-x}La_xMnO_3$ with $x = 0.10, 0.13, 0.17, 0.20$, the HT θ_D are close to the reported value of 650 K [49]. It is to be noted from table 3 that the Debye temperatures of electron doped compounds are less than the Debye temperature of $CaMnO_3$ and in turn it can be predicted that the specific heat of electron doped compounds is higher. It can also be observed from table 3 that the Debye temperature decreases smoothly with increasing electron doping or increased electron concentration in the e_g orbital. These theoretical values of lattice thermal properties can serve as a guide to experimental workers in the future. The Debye temperatures estimated from high temperature analysis of the lattice specific heat in the paramagnetic phase and other thermal properties of the electron doped manganites are reported in table 4, and compared with the available earlier reports in table 4. The results on cohesive properties indicate enhanced stability of the paramagnetic phase at elevated temperatures. The bulk modulus of these compounds is higher in the paramagnetic phase due to the linearly increasing lattice distortions in this phase compared to the spin ordered phase. Further, the reststrahlen frequency is higher in this phase and it gives higher Debye temperature in the paramagnetic phase for all electron doped compounds. In turn, the lattice specific heat of this phase is expected to reduce. If we compare the Debye temperatures of $x = 0.20$ doped compounds, then tetravalently doped compounds have somewhat lesser values of the Debye temperature compared to the trivalently doped compounds. The same can be observed for other doping concentrations (tables 3 and 4). The Grüneisen parameter is above 3 for most of the compounds in the paramagnetic phase, which indicates the enhanced anharmonic effects in this temperature regime.

3.5. Specific heat

Now, to start the systematic investigations of the specific heat, we divide the case of rare earth cation doping at the A-site in $CaMnO_3$ into two categories:

(a) when the doped ion radius is smaller and
(b) when the doped ion radius is larger than that of the parent Ca^{2+} ion.

Doping at the A-site with smaller $Ln^{3+/4+}$ cations (Ce^{4+}, Nd^{3+}, Th^{4+}) in $CaMnO_3$ will favour increased buckling and reduction in the Mn–O–Mn angle. Lattice distortions will increase as the angle of rotation and tilt of the octahedra increases. This type of doping will introduce large distortions in the lattice and this effect will further accentuate with increase of temperature. The low temperature (LT) bulk modulus (below the magnetic transition temperature) is observed to be different from the high temperature (HT; far above T_c/T_N) bulk modulus in our investigation. The Debye temperature used for calculating the low temperature specific heat is quite different from the Debye temperature at which the specific heat reaches its saturation value. Similar findings were reported earlier also. To illustrate, it is clear from our earlier investigations on $LaMnO_3$ that the Debye temperature is dependent on the temperature and its value at high temperature is more than the value at low temperatures [11]. It is also established that, for compounds whose low temperature (LT) Debye temperature is different from the high temperature (HT) Debye temperature, a Debye model with one Debye temperature (LT) does not account for all of the specific heat, as the contribution of optical phonons at higher temperature cannot be neglected and some other formulation such as the Einstein model is needed to account for the specific heat at higher temperatures.

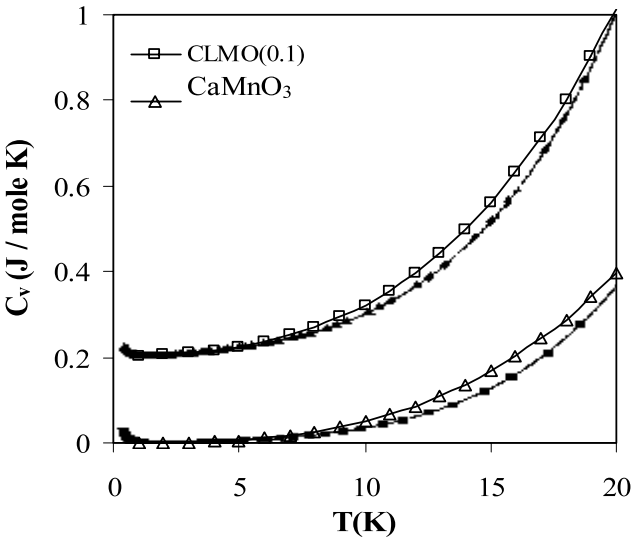

Figure 5. Specific heat of $CaMnO_3$ (open triangles with line), $La_{0.1}Ca_{0.9}MnO_3$ (open squares with line) and experimental data (solid symbols) of Cornelius *et al* [49].

Experimentally it is observed that the superexchange angle Mn–O–Mn increases with increasing external pressure and a similar effect can be observed by increasing the average cation size at the A-site (substitution with a larger cation) in $CaMnO_3$. In the case of larger cation (La^{3+}, Bi^{3+}) doping at the A-site in $CaMnO_3$ manganites, this effect of doped cation size on the superexchange angle can be observed. The increasing Mn–O–Mn angle will straighten the cell edges and reduce the lattice distortions. Thus the lattice distortions are reduced in such doped compounds, the effect of distortions on the bulk modulus will be less and the Debye temperature extracted from the low temperature specific heat will be quite similar to the Debye temperature at which the specific heat reaches its saturation value. Such solids can be thought of as Debye solids [43].

On the basis of above discussion we have calculated the specific heat for $CaMnO_3$ and $Ca_{0.9}La_{0.1}MnO_3$ over the temperature range 0 K $\leqslant T \leqslant$ 20 K and the results are displayed in figure 5. The low temperature specific heat of $CaMnO_3$ and $La_{0.1}Ca_{0.9}MnO_3$ is compared with the experimental data of Cornelius *et al* [49] and the match is found to be satisfactory. Our calculated values of the low temperature specific heat for $CaMnO_3$ and $La_{0.1}Ca_{0.9}MnO_3$ are slightly

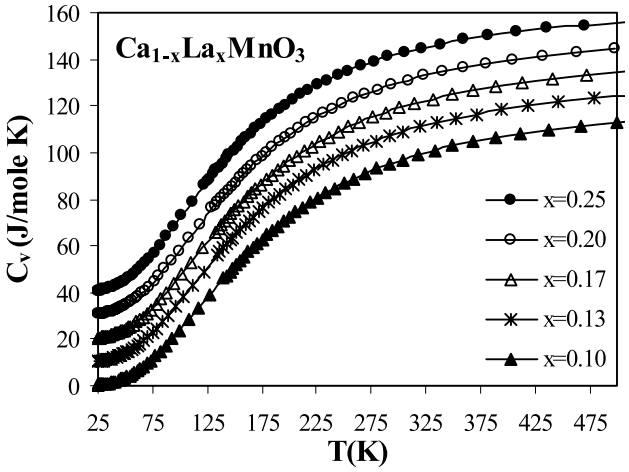

Figure 6. Lattice specific heat of the electron doped compound $Ca_{1-x}La_xMnO_3$ in the 25 K $< T <$ 500 K temperature interval. The curves for $x = 0.13, 0.17, 0.20, 0.25$ are shifted upward by 10 J, 20 J, 30 J, 40 J respectively from the $x = 0.10$ curve for clarity. The curve for $x = 0.10$ is undisplaced.

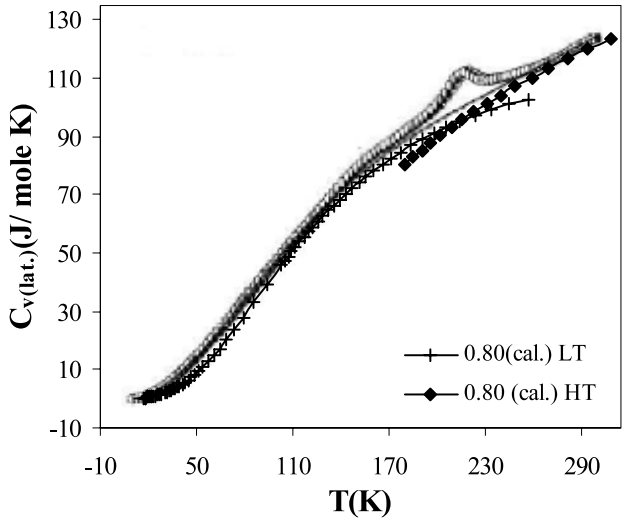

Figure 7. Lattice specific heat of $Ca_{0.8}La_{0.2}MnO_3$ (cross with line) predicted in the antiferromagnetic region below the magnetic transition temperature T_N and its comparison with the experimental curves for $Ca_{0.75}La_{0.25}MnO_3$ of Zheng *et al* [50]. Also shown is the calculated specific heat (solid square with line) predicted for the paramagnetic region (above T_N).

higher than the experimental values, which indicates that our model has slightly underestimated the Debye temperature at lower temperatures. Here, the calculated specific heat values in the lower temperature region of $T < (\theta_D/50)$ are estimated with the help of (9).

Further, the specific heat of electron doped compounds is calculated with (8), varying the temperature in the range 10 K $< T <$ 500 K, and the results are displayed for $Ca_{1-x}La_xMnO_3$ representative compounds in figure 6 for 25 K $< T <$ 500 K. These values are compared with the available experimental data in subsequent figures. In figure 7 the specific heat of $Ca_{0.8}La_{0.2}MnO_3$ can be compared with the experimental curves for $Ca_{0.75}La_{0.25}MnO_3$ given by Zheng

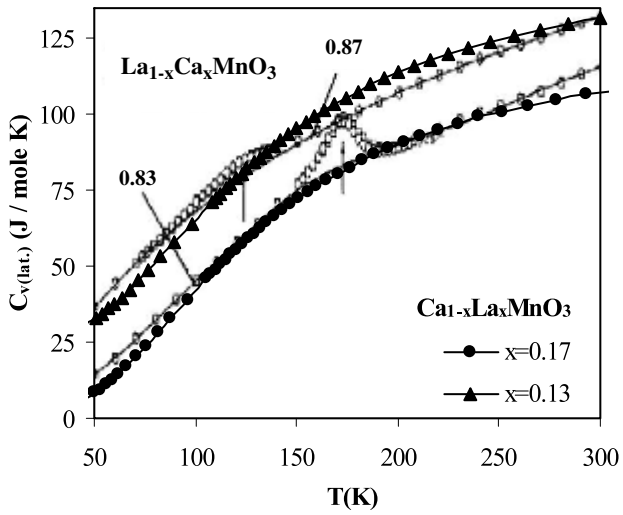

Figure 8. The lattice specific heat of $Ca_{0.83}La_{0.17}MnO_3$ (solid circle with line) and $Ca_{0.87}La_{0.13}MnO_3$ (solid triangle with line) calculated with the LT Debye temperature is compared with the experimental specific heat curves of Qian *et al* [51] (open squares and circles with line). The calculated as well as the experimental curves for $Ca_{0.87}La_{0.13}MnO_3$ have been shifted upward by 25 J for clarity.

et al, due to the lack of experimental data at the same doping parameter [50]. The specific heat calculated with the LT Debye temperature (table 3) in the antiferromagnetic phase of the compound (below T_N) shows a satisfactory match. Above T_N the specific heat estimation using the HT Debye temperature (table 3) is not so good but the trend of variation of specific heat is similar to that for the experimentally observed data. The observed peak in the experimental curves around T_C can be reproduced in the calculated values by adding the contribution due to ferromagnetic spin wave interactions and additional specific heat due to charge ordering, which was not estimated in the present work. The estimation of these contributions is beyond the scope of the present model potential.

Figure 8 shows the temperature dependence of the specific heat of $Ca_{0.83}La_{0.17}MnO_3$ and $Ca_{0.87}La_{0.13}MnO_3$ and the comparison with the experimental specific heat curves of Qian *et al* [51]. The match of the specific heat values using the LT Debye temperatures of 528 K and 540 K for $x = 0.17$ and $x = 0.13$ respectively is however not very satisfactory, but our calculated values for the specific heat are more or less near the experimental curves and the peak observed in the experimental specific heat curves at ∼175 K due to A-type AF ordering could not be observed in the calculated curves. The difference can be attributed to non-inclusion of the magnetic spin wave (C_m) and charge ordering (C') contributions to the specific heat. It is well known that the specific heat of Ln doped $CaMnO_3$ at low temperatures in the electron doped region of the phase diagram is

$$C_v = C_{v(\text{lattice})} + C_m + C' \tag{22}$$

where the first term is the lattice contribution which constitutes the major part of the specific heat and is calculated by us using the MRIM, the second term is the ferromagnetic spin wave contribution effective below the magnetic transition

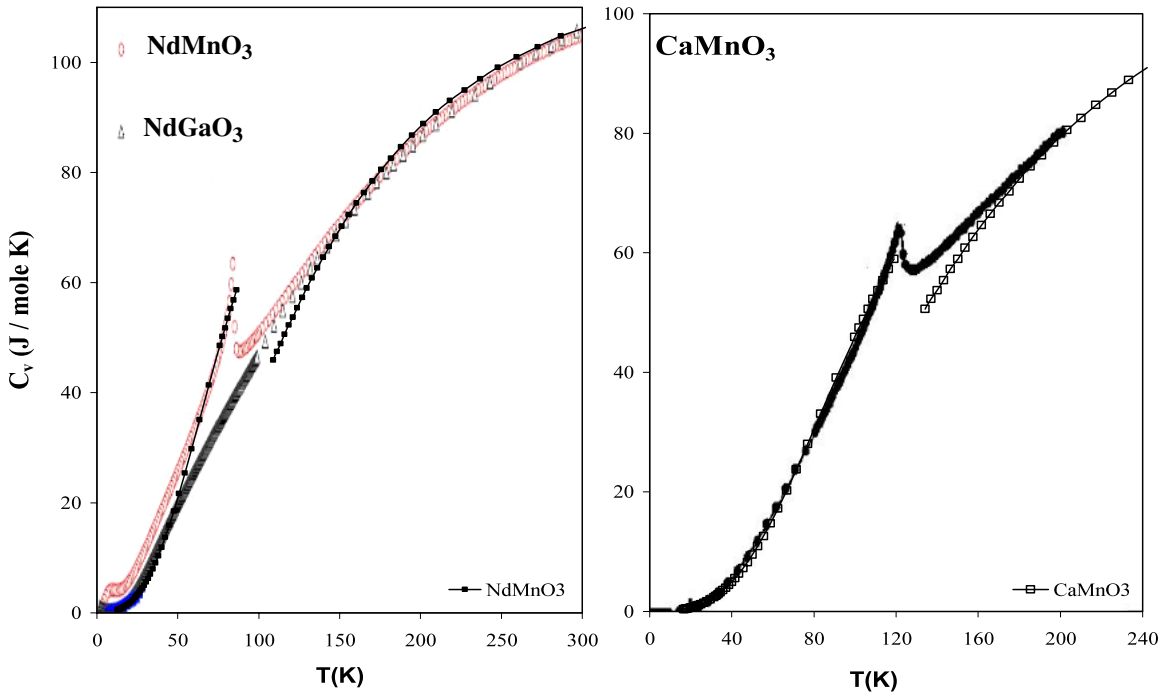

Figure 9. Lattice specific heat of $NdMnO_3$ and $CaMnO_3$, using two Debye temperatures in the antiferromagnetic phase (below T_N) and paramagnetic phase (above T_N), and the comparison of calculated values with experimental data of Berggold *et al* [52] and Moritomo *et al* [53].

(This figure is in colour only in the electronic version)

temperature only and the last term is the specific heat due to excess entropy observed in the charge ordered systems.

The value of the ferromagnetic spin wave contribution to the specific heat C_m can be calculated from the following expression:

$$C_m = 0.113 V k_B \left[\frac{k_B}{D}\right]^{1.5} T^{3/2} \qquad (23)$$

where V is the molar volume, k_B is Boltzmann's constant and D is the spin wave stiffness constant.

The lattice specific heat results obtained using two Debye temperatures (above and below T_N) are given in figure 9 for $NdMnO_3$ and $CaMnO_3$, and the comparison with the experimental data of Berggold *et al* [52] and Moritomo *et al* [53] is also shown in the same figure. The Debye temperature of these compounds below T_N is found to be different from the stable room temperature paramagnetic phase values. Hence the two-Debye-temperature model, for above and below the magnetic transition temperature, can predict the lattice specific heat satisfactorily over a broader range of temperature. The present results indicate that the spin ordered phase is less distorted and has higher compressibility as compared to the paramagnetic phase for these electron doped compounds. The specific heat of the compound is more in the ordered phase compared to the paramagnetic phase. Figure 10 shows the calculated specific heat of $CaMnO_3$ with one Debye temperature and its comparison with experimental curves of Moritomo *et al* [53]. It is clear from figure 10 that the values calculated with one HT Debye temperature do not give a satisfactory match below T_N.

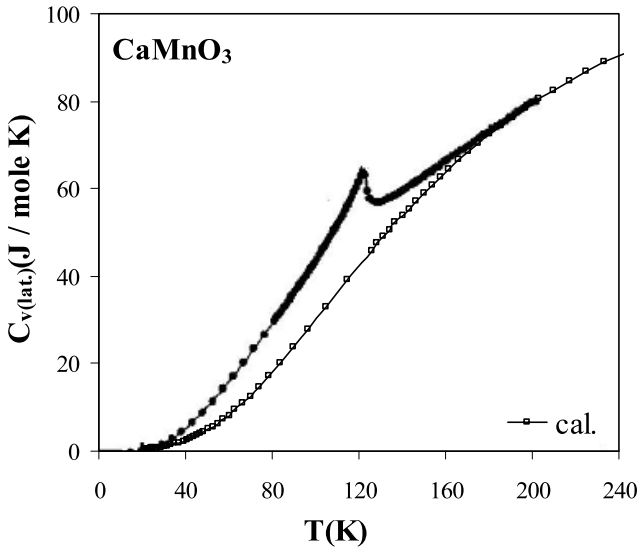

Figure 10. Lattice specific heat of $CaMnO_3$ predicted with the HT Debye temperature (open circle with line) and its comparison with data of Moritomo *et al* [53] (solid circle with line).

4. Conclusion

We studied $CaMnO_3$ substituted with trivalent (Ln = La, Pr, Nd, Bi) and tetravalent (Ce, Th) cations at the A-site as regards its thermal properties and the effect of various lattice distortions on these properties.

On the basis of the overall discussion, it may be concluded that the modified rigid ion model (MRIM) is capable of

giving a satisfactory prediction of the thermal properties of electron doped $CaMnO_3$. We have found that in electron doped materials, the Debye temperature decreases with increasing electron doping. The specific heat correspondingly increases with increasing electron doping level. The decrease in θ_D indicates that an anomalous softening of the lattice or increase in the T^3 term in the specific heat occurs with increase of the electron doping. Our results are probably the first reports of the lattice specific heat at these temperatures and compositions. We have also reproduced the various lattice distortions and their relation to elastic properties systematically, and then that to the thermal properties of the lattice. In the insulating paramagnetic state, distortions of the Mn–O environment are linear with calcium concentration. In the low temperature ferromagnetic/spin ordered state, at least 50% of the distortion is removed due to spin ordering. The findings indicate that strong coupling between spin and lattice degrees of freedom exists in these electron doped materials. The results are in satisfactory agreement with the previous reports. A sharp peak can be seen in figures 9 and 10 in the experimental curves at their respective Néel temperatures due to spin interactions. This feature cannot be revealed in the calculated curves by our present MRIM.

We demonstrate that the electron concentration, size mismatch and JT effects are the dominant factors, whereas the charge mismatch and buckling of the Mn–O–Mn angle influence the thermal properties to a lesser degree. The Debye temperature of these compounds below T_N is found to be different from the stable room temperature paramagnetic phase values. We also propose a two-Debye-temperature model for above and below the magnetic transition temperature which can predict the lattice specific heat satisfactorily over a broader range of temperature.

Thus, the successful exposition of the temperature-dependent thermal properties of electron doped $Ca_{1-x}Ln_xMnO_3$ (Ln = La, Ce, Pr, Nd, Th, Bi) attained by us is remarkable in view of the inherent simplicity and less parametric nature of the modified rigid ion model (MRIM). Present results on specific heat could be further improved by incorporating the effect of the interactions due to spin wave and charge ordering contributions within the Debye approach.

Acknowledgments

The authors are grateful to the University Grants Commission (UGC), New Delhi, for providing financial support. One of us (Archana Srivastava) is grateful to UGC, New Delhi, for providing a Teacher Fellowship.

References

[1] Murakami Y, Shindo D, Chiba H, Kikuchi M and Syono Y 1997 *Phys. Rev.* B **55** 15043–7
Murakami Y, Shindo D, Chiba H, Kikuchi M and Syono Y 1999 *Phys. Rev.* B **59** 6395–9
Chiba H, Kikuchi M, Kusaba K, Muraoka Y and Syono Y 1996 *Solid State Commun.* **99** 499–502
[2] Martin C, Maignan A, Damay F, Hervieu M and Raveau B 1997 *J. Solid State Chem.* **134** 198–202
[3] Zeng Z, Greenblatt M and Croft M 2001 *Phys. Rev.* B **63** 224410
[4] Maignan A, Martin C, Damay F and Raveau B 1998 *Chem. Mater.* **10** 950–4
[5] Yakel H L 1955 *Acta Crystallogr.* **8** 394–8
[6] Wollan E O and Koehler W C 1955 *Phys. Rev.* **100** 545–63
[7] Hervieu M, Martin C, Maignan A, Van Tendeloo G and Raveau B 1999 *Eur. Phys. J.* B **10** 397–408
[8] Hafemeister D W and Flygare W H 1965 *J. Chem. Phys.* **43** 795–800
[9] Pauling L 1945 *Nature of the Chemical Bond* (Ithaca, NY: Cornell University Press)
[10] Slater J C and Kirkwood J G 1931 *Phys. Rev.* **37** 682–97
[11] Rini E G, Rao M N, Chaplot S L, Gaur N K and Singh R K 2007 *Phys. Rev.* B **75** 214301
[12] Gaur N K, Choithrani R and Srivastava A 2008 *Solid State Commun.* **145** 308–11
[13] Choithrani R and Gaur N K 2007 *J. Magn. Magn. Mater.* **320** 612–6
[14] Kaur N, Mohan R, Gaur N K and Singh R K 2007 *Physica* C **451** 24–30
Kaur N, Mohan R, Gaur N K and Singh R K 2007 *J. Phys. Chem. Solids* **68** 2247–51
[15] Srivastava A, Gaur N K, Kaur N and Singh R K 2008 *J. Magn. Magn. Mater.* **320** 2596–601
[16] Li X G, Zheng R K, Li G, Zhou H D, Huang R X, Xie J Q and Wang Z D 2002 *Europhys. Lett.* **60** 670–6
[17] Markovich V, Fita I, Puzniak R, Rozenberg E, Martin C, Wisniewski A, Yuzhelevski Y and Gorodetsky G 2005 *Phys. Rev.* B **71** 134427–32
[18] Llobet A, Frontera C, Garcıa-Munoz J L, Ritter C and Aranda M A G 2000 *Chem. Mater.* **12** 3648–57
[19] Zheng R K, Li G, Yang Y, Tang A N, Wang W, Qian T and Li X G 2004 *Phys. Rev.* B **70** 014408–14
[20] Caspi E N, Avdeev M, Short S, Jorgensen J D, Lobanov M V, Zeng Z, Greenblatt M, Thiyagarajan P, Botez C E and Stephens P W 2004 *Phys. Rev.* B **69** 104402
[21] Melo Jorge M E, Nunes M R, Silva Maria R and Sousa D 2005 *Chem. Mater.* **17** 2069–75
[22] Santhosh P N, Arulraj A, Vanitha P V, Singh R S, Sooryanarayana K and Rao C N R 1999 *J. Phys.: Condens. Matter* **11** L27–33
[23] Alonso J A, Martínez-Lope M J, Casais M T and Fernández-Díaz M T 2000 *Inorg. Chem.* **39** 917–23
[24] Vegard L 1921 *Z. Phys.* **5** 17–26
[25] Kovaleva N N, Gavartin J L, Shluger A L and Stoneham A M 2002 *Physica* B **312/313** 734–6
De Souza R A, Saiful Islam M, Boris A V and Ivers-Tiffe Ellen 1999 *J. Mater. Chem.* **9** 1621–7
[26] Liu D, Zhang S and Wu Z 2003 *Inorg. Chem.* **42** 2465–9
[27] Glasser L 1995 *Inorg. Chem.* **34** 4935–6
[28] Nikiforov A E, Popov S E and Shashkin S Yu 2000 *Physica* B **276** 772–3
[29] Buch J J U, Lalitha G, Pathak T K, Vasoya N H, Lakhani V K, Reddy P V, Kumar R and Modi K B 2008 *J. Phys. D: Appl. Phys.* **41** 025406
[30] Loa I, Adler P, Grzechnik A, Syassen K, Schwarz U, Hanfland M, Rozenberg G Kh, Gorodetsky P and Pasternak M P 2001 *Phys. Rev. Lett.* **87** 125501
[31] Fuks D, Dorfman S, Felsteiner J, Bakaleinikov L, Gordon A and Kotomin E A 2004 *Solid State Ion.* **173** 107–11
[32] Tang F L and Zhang X 2007 *Comput. Mater. Sci.* **40** 434–8
[33] Trimarchi G and Binggeli N 2005 *Phys. Rev.* B **71** 035101
[34] Markovich V, Fita I, Puzniak R, Rozenberg E, Martin C, Wisniewski A, Maignan A, Raveau B, Yuzhelevskii Y and Gorodetsky G 2004 *Phys. Rev.* B **70** 024403
Pinsard-Gaudart L, Rodríguez-Carvajal J, Daoud-Aladine A, Goncharenko I, Medarde M, Smith R I and Revcolevschi A 2001 *Phys. Rev.* B **64** 064426
[35] Martín Pendás A, Costales A, Blanco M A, Recio J M and Luanã V 2000 *Phys. Rev.* B **62** 13970–8

[36] Shannon R D 1976 *Acta Crystallogr.* A **32** 751–67
[37] Kittel C 1976 *Introduction to Solid State Physics* 5th edn (New York: Wiley) www.webelements.com
[38] Zhu C and Zheng R 2000 *J. Appl. Phys.* **87** 3579–81
[39] Loa I, Syassen K, Wang X, Lichenberg F, Hanflad M and Kurtscher C A 2004 *Phys. Rev.* B **69** 224105
[40] Kozlenko D P, Dubrovinsky L S, Savenko B N, Voronin V I, Kiselev E A and Proskurnina N V 2008 *Phys. Rev.* B **77** 104444
[41] Zimmer H G, Winzen H and Syassen K 1985 *Phys. Rev.* B **32** 4066–70
Shein I R and Ivanovskii A L 2008 *J. Phys.: Condens. Matter* **20** 415218
[42] Zhou J-S and Goodenough J B 2003 *Phys. Rev.* B **68** 054403
[43] Anderson O L 1998 *Am. Mineral.* **83** 23–35
[44] Radaelli P G and Cheong S-W 2002 *Phys. Rev.* B **66** 094408
[45] Fedorov I, Lorenzana J, Dore P, De Marzi G, Maselli P, Calvani P, Cheong S-W, Koval S and Migoni R 1999 *Phys. Rev.* B **60** 11875–8
[46] Woodfield B F, Wilson M L and Byers J M 1997 *Phys. Rev. Lett.* **78** 3201–4
[47] Ghivelder L, Abrego Castillo I, Gusmaõ M A, Alonso J A and Cohen L F 1999 *Phys. Rev.* B **60** 12184–90
[48] Talati M and Jha P K 2006 *Comput. Mater. Sci.* **37** 64–8
[49] Cornelius A L, Light B E and Neumeier J J 2003 *Phys. Rev.* B **68** 014403
[50] Zheng R K, Tang A N, Yang Y, Wang W, Li G, Li X G and Ku H C 2003 *J. Appl. Phys.* **94** 514–8
[51] Qian T, Zheng R K, Zhang T, Zhou T F, Wu W B and Li X G 2005 *Phys. Rev.* B **72** 024432
[52] Berggold K, Baier J, Meier D, Mydosh J A, Lorenz T, Hemberger J, Balbashov A, Aliouane N and Argyriou D N 2007 *Phys. Rev.* B **76** 094418
[53] Moritomo Y, Machida A, Nishibori E, Takata M and Sakata M 2001 *Phys. Rev.* B **64** 214409
[54] Youn S J and Min B I 1998 *J. Korean Phys. Soc.* **32** 576–83
[55] Hase I and Yanagisawa T 2007 *Phys. Rev.* B **76** 174103